Optica Applicata, Vol. LV, No. 1, 2025
DOI: 10.37190/oa/200186

Simulation of mushroom-typed modified near-ballistic uni-traveling-carrier photodetector with sub-THz operational bandwidth

Yuansen Shen[1,2,3], Huijuan Niu[1,2,*], Qingtao Chen[4], Liwen Wang[1,2,3], Kai Liu[3], Xiaofeng Duan[3], Yongqing Huang[3]

[1]School of Physics Science and Information Technology, Liaocheng University, Liaocheng 252059, China

[2]Shandong Provincial Key Laboratory of Optical Communication Science and Technology, Liaocheng University, Liaocheng 252000, China

[3]State Key Laboratory of Information Photonics and Optical Communications, Beijing University of Posts and Telecommunications, Beijing 100876, China

[4]Department of Electrical Engineering, Poly-Grames Research Center, Polytechnique Montréal, Montréal H3T 1J4, Canada

[*]Corresponding author: supernhj@lcu.edu.cn

We report a novel mushroom-typed modified near-ballistic uni-traveling-carrier photodetector (modified NBUTC-PD) based on a drift-diffusion model which achieves high responsivity at the sub-THz regime. By well-designed active and depleted regions to form a "mushroom" type, with the optimal cliff and charge layers to make electrons transport at a "near-ballistic" speed, of order 10^7 cm/s, as well as the rational hybrid-doping absorber, the modified NBUTC-PD successfully achieves the decoupling between the bandwidth and responsivity characteristics. For the modified NBUTC-PD with an active area of 12.56 μm^2, the simulation shows that the 3-dB bandwidth is up to 107 GHz, with a responsivity up to 0.38 A/W, at a reverse bias voltage of 1 V. The decrease in 3-dB bandwidth of the modified NBUTC-PD is analysed in detail under high-light injection conditions, which results from the energy band shift and electric field collapse.

Keywords: uni-traveling-carrier photodetector, mushroom-typed photodetector, near-ballistic transport, high responsivity, high-speed operation.

1. Introduction

As optical fiber communications technology continues to advance and the demand for greater transmission capacity grows, wireless and bandwidth are becoming two of the most important trends in modern communication systems [1-3]. Due to the limitation

of bandwidth, it is not easy to achieve high-speed and high efficiency media services. The core components of optical fiber communication systems include optical transmitters, repeaters, and optical receivers, *etc*. [4]. The photodetector, as one component of the optical receivers, is often used to perform the conversion between the optical and electrical signals. Meanwhile, photodetectors with high bandwidth, high quantum efficiency, high saturation, and high output power usually meet the system requirements. However, the traditional PIN photodetector also has three serious drawbacks: trade-off between the bandwidth and responsivity, transit time and RC time constant limited bandwidths, and hole drift speed constraints on device response [5,6]. Therefore, it is necessary to design a novel photodetector to overcome the drawbacks of PIN photodetectors.

To tackle the above-mentioned problems of the conventional photodetectors, ISHIBASHI *et al*. proposed a uni-traveling-carrier photodetectors (UTC-PDs), which only allows electrons to be transported as the active carriers, effectively improving the bandwidth and saturation current of the device [7,8]. Since then, UTC-PDs have become a hot spot in photodetector research due to their excellent performance. In 2006, WU *et al*. proposed a near-ballistic uni-traveling-carrier photodetectors (NBUTC-PD), which improves the performance of the device by adding a lightly doped charge layer at the back-end of the collector, resulting in a high saturation current-bandwidth product of 1280 mA-GHz and a responsivity of 1.14 A/W [9]. In 2008, the group also proposed an NBUTC-PD with a collector thickness of 410 nm and an active area of 64 μm^2, achieving a transit time-limited bandwidth of 400 GHz and a saturation current-bandwidth product of 2952 mA-GHz [10]. In 2010, LI *et al*. proposed two back-illuminated high-power uni-traveling-carrier photodetector with a cliff layer structure (MUTC-PD), in which a higher doping concentration of the cliff layer and a thinner absorber were taken in the device, achieving 3-dB bandwidths of 24 GHz at diameters of 34 μm [11]. In 2021, Xiong's group proposed a novel uni-traveling-carrier photodetector with a double drift layer, which achieved a bandwidth of 105 GHz and a responsivity of 0.17 A/W [12]. In 2023, Huang's group proposed a cascaded array structure for the UTC-PD, which can effectively reduce the overall capacitance of the device and achieve an increase of the 3-dB bandwidth from 203 to 255 GHz [13]. In 2024, HUANG *et al*. proposed an undercut collector structure to alleviate the mutual constraints between UTC-PD responsivity and saturation power, and finally achieved a 3-dB bandwidth of 220 GHz with a 3 μm wide undercut collector profile [14].

In this paper, a mushroom-typed modified near-ballistic uni-traveling carrier photodetector (modified NBUTC-PD) with high speed and high responsivity is designed with drift-diffusion model and simulated by ATLAS of Silvaco TCAD. The design of mushroom-mesa structure [15-23] can effectively calibrate the junction capacitance of the device and reduce the influence of RC time constant limited bandwidth to improve the bandwidth. In our design, the layer structure of conventional UTC-PD [24] is optimized as well as employing Gaussian-graded doping and unintentionally doped absorbers [25], which can make it possible to obtain a high bandwidth along with a high responsivity (*i.e.* quantum efficiency). Note that the layer structure in our design follows

a vertical configuration, while most of the parameters are taken from [24]. The optimized cliff layer and the charge layer enable carriers to transport in velocity overshoot, which can effectively enhance the electric field of the depletion layer and weaken the space charge effect. Simulation results show that the bandwidth and responsivity of the modified device can reach 107 GHz and 0.18 A/W (up to 0.38 A/W with optical power exceeding 20 mW) at a reverse bias voltage of 1 V for an active area of 12.56 μm^2. Finally, the physical mechanisms of bandwidth reduction and current saturation at high power were deeply explored from the perspectives of energy band and electric field, and it was found that high-power energy band offset and electric field collapse for intrinsic reasons. This type of modified NBUTC-PD with high bandwidth and high responsivity could have potential applications in THz electric [26,27], photonic [28] or hybrid electronic–photonic [29] transmitter and receiver [30] systems.

2. Device structure design and optimization

2.1. Optimization of absorbers

The modified NBUTC-PD layer structure is shown in Table 1.

In terms of doping for absorber, the traditional highly doped mechanism is replaced with a partially depleted doping. Moreover, the middle two layers of the partially depleted layer are doped using a Gaussian gradient doping profile [31,32]. This creates a larger potential and electric field in the absorber and improves the bandwidth of the device. In addition, the introduction of unintentionally doped absorbers can also improve the quantum efficiency of UTC-PDs [33-35].

Considering the thickness of absorber, the variation curves of bandwidth and responsivity of conventional UTC-PD are also investigated, as shown in Fig. 1(a). The specific simulation method is to gradually change the thickness of the middle two absorbers while keeping their thickness values the same. It can be seen that with increasing thickness

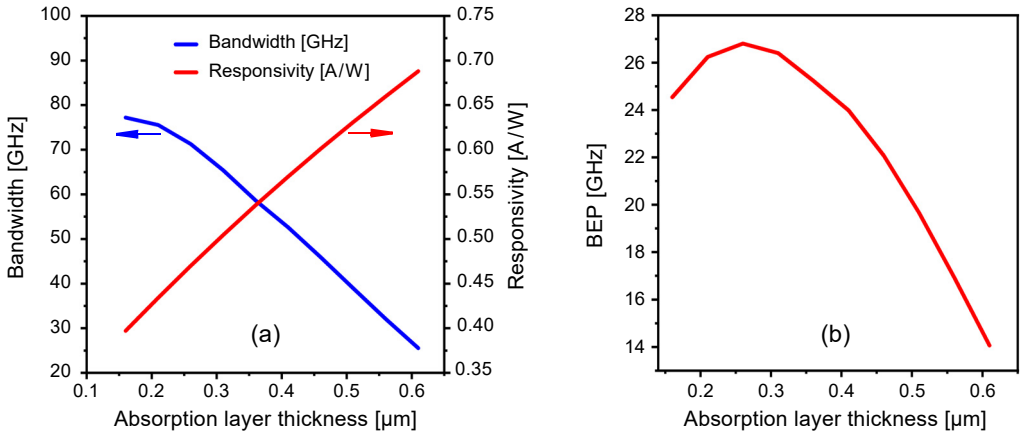

Fig. 1. (a) Variation curves of bandwidth and responsivity with thickness of the absorber (*i.e.* absorption layer). (b) The thickness of absorber *versus* BEP.

T a b l e 1. The conventional UTC-PD [24] and modified NBUTC-PD layer structures.

		UTC-PD		Modified NBUTC-PD	
Layers	Material	Doping [cm^{-3}]	Thickness [nm]	Doping [cm^{-3}]	Thickness [nm]
P-contact	$In_{0.53}Ga_{0.47}As$	2×10^{19}	50	2×10^{19}	50
Barrier	InP	2×10^{18}	100	2×10^{19}	200
Grading	$In_{0.85}Ga_{0.15}As_{0.32}P_{0.68}$	2×10^{18}	10	2×10^{18}	10
Grading	$In_{0.66}Ga_{0.34}As_{0.73}P_{0.27}$	2×10^{18}	10	2×10^{18}	10
Absorber	$In_{0.53}Ga_{0.47}As$	2×10^{18}	50	2×10^{18}	50
	$In_{0.53}Ga_{0.47}As$	1×10^{18}	90	Gaussian doping (2×10^{17}, char = 0.15)	90
	$In_{0.53}Ga_{0.47}As$	5×10^{17}	90	Gaussian doping (7×10^{16}, char = 0.15)	90
	$In_{0.53}Ga_{0.47}As$	1×10^{16}	30	9×10^{16}	30
Spacer	$In_{0.66}Ga_{0.34}As_{0.73}P_{0.27}$	1×10^{16}	10	1×10^{17}	10
Spacer	$In_{0.85}Ga_{0.15}As_{0.32}P_{0.68}$	1×10^{16}	10	1×10^{17}	10
Cliff	InP	3×10^{17}	30	5×10^{18}	10
Collector/drift	InP	1×10^{16}	300	1×10^{16}	100
Charge	InP	—	— 5	1×10^{18}	
Suffer	InP	—	—	1×10^{15}	100
Buffer	InP	1×10^{18}	100	—	—
N-contact	InP	1×10^{19}	1000	1×10^{19}	1000
		Semi-insulating-InP substrate			

of the absorber the device bandwidth gradually decreases while its responsivity gradually increases. This behavior is also consistent with the theoretical analysis [36,37]. The variation curve of bandwidth efficiency product (BEP = bandwidth × quantum efficiency) with the thickness of the absorber is shown in Fig. 1(b). To balance the trade-off between the high-speed response and high saturation [38], an absorber thickness of 260 nm is selected, as it corresponds to the maximum BEP.

2.2. Optimization of the cliff layer

The cliff layer is generally found between the InGaAs absorber and the InP collector, which is used to enhance the electric field at the heterojunction interface, allowing for faster carrier transport and increased device bandwidth [39]. In our design, we keep the cliff thickness as a constant, while only calibrate the doping concentration and observe the variations of the 3-dB bandwidth. The doping of the cliff layer *versus* the bandwidth is given in Fig. 2. It can be seen that the 3-dB bandwidth of the device increases with the increase of the doping concentration of cliff layer until the doping concentration is up to 5×10^{18} cm^{-3}. Meanwhile, the 3-dB bandwidth of the device starts to decrease with increasing doping concentration when the doping concentration is greater than 5×10^{18} cm^{-3}. The maximum 3-dB bandwidth of the device occurs at the doping concentration of the cliff layer 5×10^{18} cm^{-3}, leading to a value of 108.66 GHz. However, it also can be seen that the lower and the higher doping concentrations of the cliff layer have little effect on the 3-dB bandwidth of the device, and the impact is biggest when the doping concentration level is 5×10^{18} cm^{-3}.

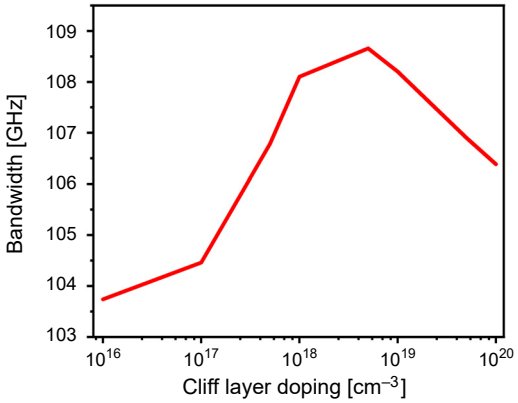

Fig. 2. The doping distribution of cliff layer *versus* the 3-dB bandwidth.

2.3. Structural parameters of the mushroom-type modified NBUTC-PD

Based on the above-mentioned considerations and optimizations, the best layer structure parameters of the modified NBUTC-PD is shown in Fig. 3. The corresponding doping concentration and layer thickness parameters are shown in Table 1. Note that

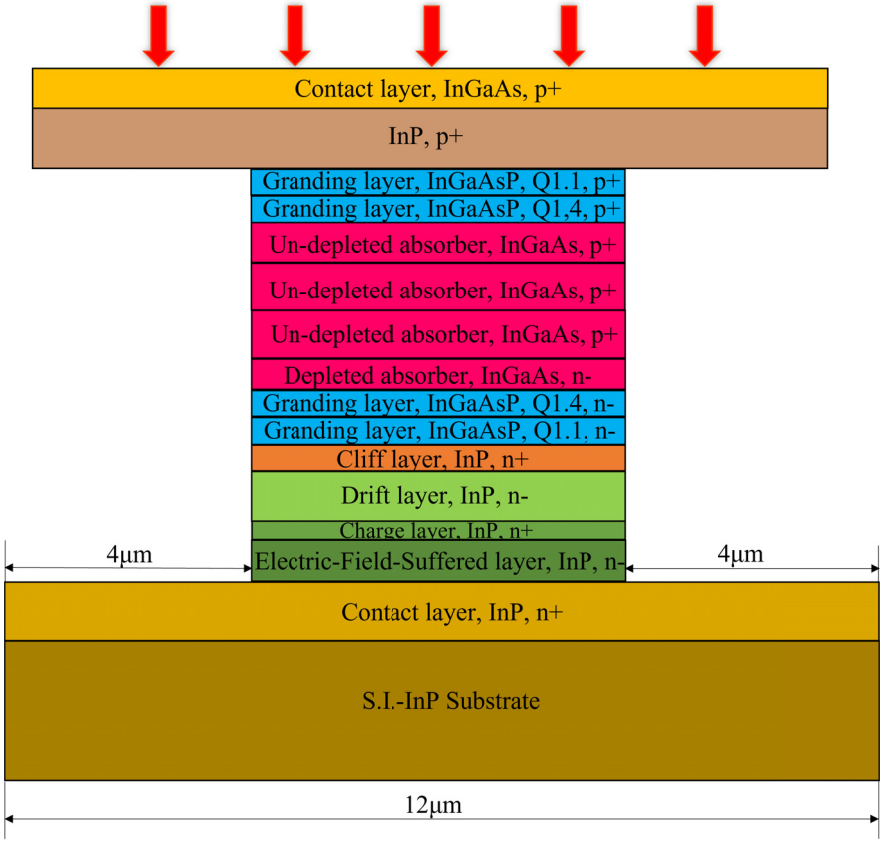

Fig. 3. Cross-section of the proposed "mushroom" typed modified NBUTC-PD.

the light can be incident either the top or bottom [11]. In this case, it was incident from the top, as illustrated in Fig. 3.

The topmost layer of the device is a p-type heavily doped $In_{0.53}Ga_{0.47}As$ contact layer, which is used here to connect to the anode and act as a good ohmic contact. Two layers of 10 nm p-doped InGaAsP are used to reduce the barrier between heterojunctions and to accelerate carrier transport [40,41]. Four graded doped absorbers are set up, and the middle two partially depleted absorbers are Gaussian doped to form a relatively large potential and electric field, so that the carriers can accelerate the movement under the action of the built-in electric field to improve the response speed of the device. The heavily doped n-type InP cliff layer is able to form a higher electric field, suppressing the charge accumulation at the heterojunction interface and obtaining a higher saturation current. The material used for the collector and the subsequent charge layer is InP, but the difference lies in the doping concentration, with the collector lightly doped with N-type and the charge layer heavily doped with N-type, which can be used to provide a high electric field in the depletion region and to maintain the peak overshoot velocity of electrons [42-44].

3. Simulation results and analysis

3.1. Responsivity and quantum efficiency

The responsivity and quantum efficiency are the most important output performance parameters in UTC-PDs. At a certain determined wavelength, the responsivity is the ratio of the output photocurrent of the photodetector to the incident optical power, and the quantum efficiency is the ratio of the number of photogenerated electron-hole pairs generated per unit time to the number of incident light quanta. Since the process of light quanta being absorbed and generating electron-hole pairs mainly occurs in the absorber, the main factors affecting the device responsivity and quantum efficiency are the thickness of the absorber and the doping concentration.

The photocurrent curves of the two photodetectors at a –1 V bias voltage are shown in Fig. 4. At low light intensity (*i.e.* optical power below 20 mW), the responsivity of both devices is measured to be 0.18 A/W. However, at higher light intensity (*i.e.* optical power exceeding 20 mW), the responsivities of the modified NBUTC-PD and UTC-PD are calculated to be 0.38 and 0.15 A/W, respectively. The corresponding quantum efficiencies are 30% for the modified NBUTC-PD and 12% for the UTC-PD. This demonstrates that the modified NBUTC-PD has a better capability for handling higher light intensity compared to the UTC-PD. Meanwhile, the responsivity of this type of modified NBUTC-PD can be enhanced by employing bottom-reflecting mirrors [45], dual-absorber structures [46], microstructures [38,47,48] high-contrast grating reflectors [49-51] or Fabry–Pérot cavity structures [52,53]. In addition, the high-speed response and responsivity also could be increased by the well-designed incident optical field distribution [54], incidence direction and contact electrode shapes [55,56].

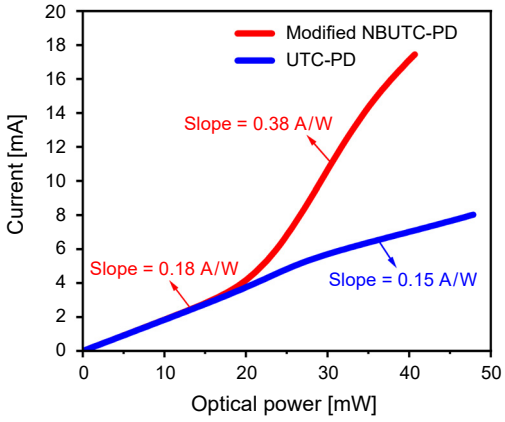

Fig. 4. The photocurrent curves of the modified NBUTC-PD and UTC-PD under a –1 V bias voltage.

3.2. High-speed response simulation

The response speed of the photodetector is an important performance parameter to measure the photoelectric conversion rate, in which the response speed can be ex-

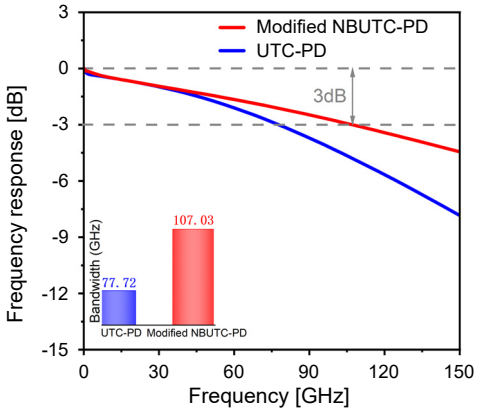

Fig. 5. Frequency response of the modified NBUTC-PD and UTC-PD under a –1 V bias voltage.

pressed in terms of 3-dB bandwidth. The larger the 3-dB bandwidth is, the larger the response speed of the photodetector is. The main factors affecting the bandwidth of the UTC-PD are: the transit time of electrons in the collector, the diffusion time of the absorber and the RC time constant.

Figure 5 shows the frequency response of the modified NBUTC-PD and UTC-PD under –1 V bias voltage. It can be seen that the 3-dB bandwidth of the modified NBUTC-PD is 107 GHz, whereas the 3-dB bandwidth of the UTC-PD is only 77 GHz. Therefore, the modified NBUTC-PD exhibits a significant increase of the 3-dB bandwidth, providing superior high-speed performance compared to non-mushroom-mesa photodetectors.

As shown in Fig. 6, we compare the junction capacitance of conventional UTC-PD, modified NBUTC-PD, and modified NBUTC-PD with undercut collector diameters of 0.8, 1.4, and 2.4 μm. From Fig. 6, it can be seen that the capacitance of modified NBUTC-PD decreases gradually with the decrease of the undercut collector diameter, and it progressively approaches the curve of the conventional UTC-PD with further

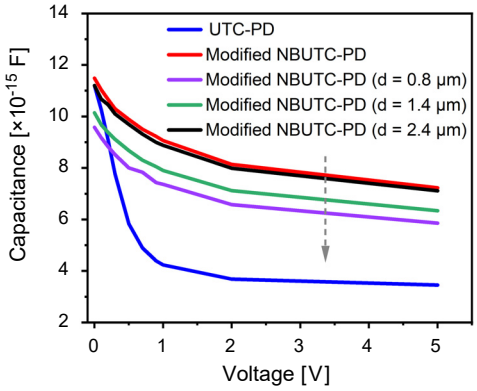

Fig. 6. Capacitance comparisons of UTC-PD and modified NBUTC-PD.

reduction in the collector diameter. Note that the key difference between UTC-PD and the modified NBUTC-PD lies in the collector thickness. The collector of the modified NBUTC-PD is thinner than that of the UTC-PD, which results in a larger junction capacitance. However, the bandwidth performance of the modified NBUTC-PD is improved due to the charge layer and the electric field suffered layer, which together enhance the electron overshoot velocity.

Near-ballistic behavior in our modified NBUCT-PDs would occur when the electrons are moving through the device with only limited scattering or energy loss. In this case, the electrons would be able to travel a significant distance through the material with almost no significant deflection or energy dissipation. This is often the result of the electrons being accelerated by a strong electric field, allowing them to travel with high velocity, like an overshot velocity, of order 10^7 cm/s. As shown in Fig. 7, the electric field distribution is obtained under a –1 V bias voltage and 500 W/cm^2 light intensity. We can find that modified NBUCT-PD generates a relatively high electric field intensity at the electric field suffered layer, which can make the carriers near-ballistic-transport with overshooting speed in the collector. Figure 8 illustrates the electron

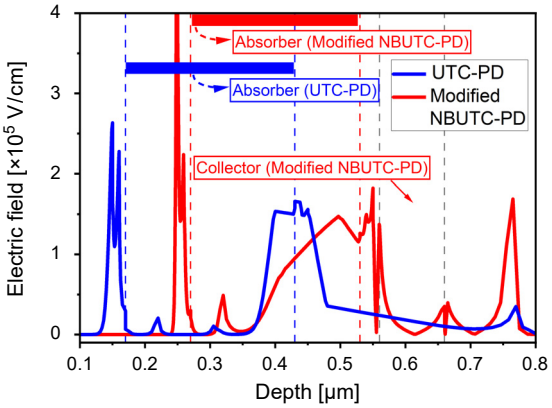

Fig. 7. Electric field of modified NBUTC-PD and UTC-PD under a –1 V bias voltage.

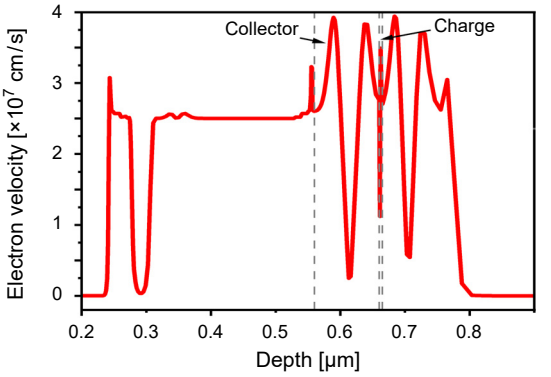

Fig. 8. Electron velocity of modified NBUTC-PD under a –1 V bias voltage.

velocity of the modified NBUTC-PD under a –1 V bias voltage. From Fig. 8, it can be obtained that the electron overshoot velocity is about 4×10^7 cm/s.

Figure 7 highlights two key differences between the modified NBUTC-PD and the UTC-PD. First, in the absorber of the modified NBUTC-PD, a strong electric field is observed at the junction between the second and third layers in absorber, likely due to the Gaussian doping in the absorber that induces this electric field. In contrast, the electric field strength in the UTC-PD is significantly weaker. Second, the average electric field in the collector of the modified NBUTC-PD is higher than that of the UTC-PD. With a reduced thickness of the collector and the presence of a high electric field, the modified NBUTC-PD achieves enhanced bandwidth and faster response speed.

3.3. The effect of optical intensity to bandwidth

Figure 9 gives the optical intensity *versus* the bandwidth. It can be found that the bandwidth increases and then decreases with the increase of incident light intensity in the range of 0 to 1×10^5 W/cm^2. The device bandwidth reaches a maximum value of 117 GHz when the incident light intensity is equal to 7×10^4 W/cm^2. The bandwidth increases because of the self-induced electric field in the absorber, which increases the drift component and accelerates the drift of electrons in the absorber. The decrease in bandwidth is due to the decrease in electric field strength due to space charge effects [57,58]. In addition, the sub-THz operational bandwidth across all optical intensity region highlights the high-response capability of our modified NBUTC-PD. This broad bandwidth indicates its potential for further applications in the THz frequency range.

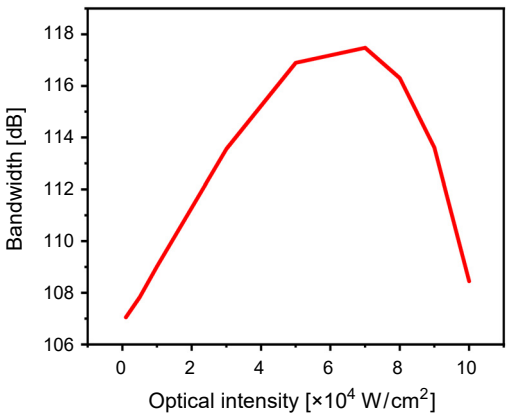

Fig. 9. Optical intensity of modified NBUTC-PD *versus* the bandwidth under a –1 V bias voltage.

The variation curves of the energy of the conduction band with different light intensities under –1 V bias voltage are shown in Fig. 10. In the absorber, the energy of the conduction band shifts down slowly with the gradual increase of the incident light intensity, which is related to the self-induced electric field generated in the absorber. At the same time, the conduction band in the absorber becomes flatter and flatter, which

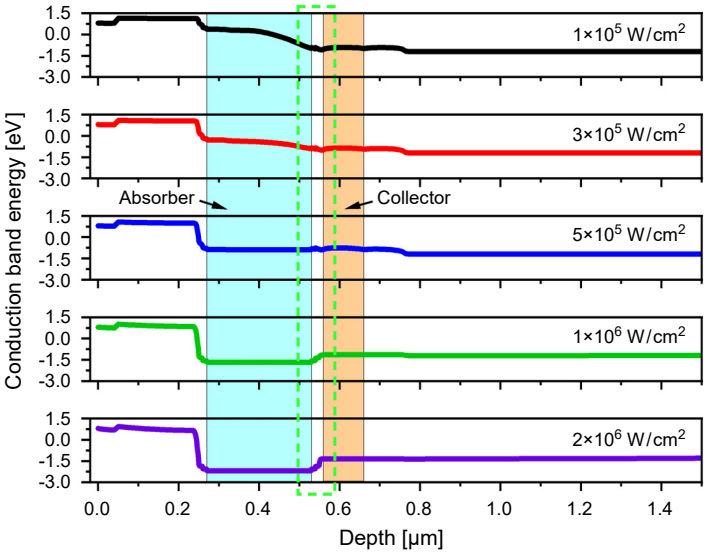

Fig. 10. Conduction band of the modified NBUTC-PD *versus* the incident light intensities under a –1 V bias voltage.

indicates that increasing the incident light intensity leads to the gradual decrease of the electric field strength in the absorber. In the collector, increasing the incident light intensity results in a change of the conduction band from concave to convex, which is because more photons are absorbed to produce more electron-hole pairs. Meanwhile, the concentration of photogenerated electrons exceeds the doping concentration of the semiconductor itself, causing the accumulation of electrons and the generation of space-charge effects.

The variation curves of the electric field strength of the modified NBUTC-PD with different light intensities under –1 V bias voltage are shown in Fig. 11. It can be seen

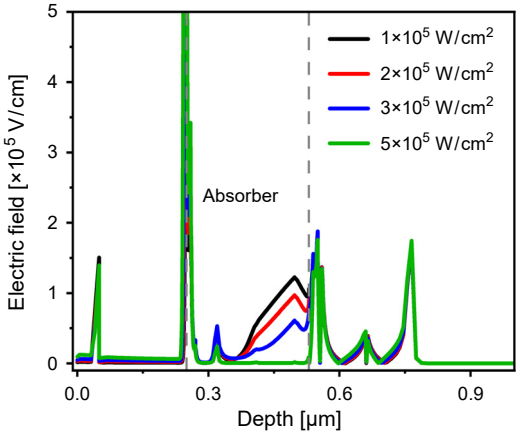

Fig. 11. Electric field of modified NBUTC-PD *versus* the optical intensity under a –1 V bias voltage.

that the effect of different light intensities on the electric field intensity of the absorber is most obvious. As the incident light intensity gradually increases from 1×10^5 to 5×10^5 W/cm^2, the slope of the corresponding curve in the absorber gradually decreases, while the peak electric field intensity gradually decreases and shifts towards the collector. Note that the electric field intensity in the absorber is approximately zero when the incident light intensity is 5×10^5 W/cm^2 [59]. It indicates that the higher incident light intensity easily causes the electric field strength of the absorber to decrease/reduce until it collapses. This reduction slows down the drift of electrons, results in the accumulation of the space charge, and ultimately leads to a decrease in both the device response and bandwidth.

4. Conclusion

In this paper, the diffusion-drift model is used to design a novel mushroom-type modified NBUTC-PD with both high speed and high quantum efficiency as well as the physical mechanism in depth. The high-speed and high-responsivity performance is achieved for the novel mushroom-type structure by optimized absorbers and introducing a cliff layer and a charge layer that enables the carriers to transport at a "near-ballistic" speed. Simulation results show that the 3-dB bandwidth of the device can reach 107 GHz while the responsivity is enhanced up to 0.38 A/W at a reverse bias voltage of 1 V for an active area of 12.56 μm^2. Moreover, the intrinsic mechanisms of bandwidth reduction is analysed from the viewpoints of between the incident light intensity *versus* the bandwidth, the conduction band, and the electric field distribution. This research lays the groundwork for addressing the "trade-off" between high response and high quantum efficiency in near-ballistic uni-traveling carrier photodetectors, potentially paving the way for advancements in sub-THz applications.

Acknowledgement
This work was funded by the Natural Science Foundation of Shandong Province (ZR2022MF305, ZR2022MF253); the Open Fund of IPOC (BUPT) (IPOC2021B07); Technology oriented small and medium-sized enterprise innovation capability enhancement project (2022TSGC2570); The 2021 Introduction and Education Plan for Young Scholars in Colleges and Universities of Shandong Province; Doctoral Scientific Research Foundation of Liaocheng University (318052168).

References

[1] GNAUCK A.H., TKACH R.W., CHRAPLYVY A.R., LI T., *High-capacity optical transmission systems*, Journal of Lightwave Technology **26**(9), 2008: 1032-1045. https://doi.org/10.1109/JLT.2008.922140
[2] XU J., SUN S.J., HU Q.G., YU J.K., LIU J.S., LUO Q., WANG W.Z., HUANG L.Y., XIANG M., WU J.J., ZHENG F.S., LI W.H., DENG L, ZHOU H.Y., ZHANG L.,JIA S.G., ZHANG X.H., CHEN H.T., *Unrepeatered transmission over 670.64 km of 50G BPSK, 653.35 km of 100G PS-QPSK, 601.93 km of 200G 8QAM, and 502.13 km of 400G 64QAM*, Journal of Lightwave Technology **38**(2), 2020: 522-530. https://doi.org/10.1109/JLT.2019.2939842
[3] ZHANG J.W., YU J.J., CHIEN H.C., *Linear and nonlinear compensation for 8-QAM SC-400G long-haul transmission systems*, Journal of Lightwave Technology **36**(2), 2018: 495-500. https://doi.org/10.1109/JLT.2017.2758326

[4] Wei J.L., Eiselt N., Griesser H., Grobe K., Eiselt M.H., Vegas Olmos J.J., Tafur Monroy I., Elbers J.P., *Demonstration of the first real-time end-to-end 40-Gb/s PAM-4 for next-generation access applications using 10-Gb/s transmitter*, Journal of Lightwave Technology **34**(7), 2016: 1628 -1635. https://doi.org/10.1109/JLT.2016.2518748

[5] Beling A., Campbell J.C., *High-speed photodiodes*, IEEE Journal of Selected Topics in Quantum Electronics **20**(6), 2014: 57-63. https://doi.org/10.1109/JSTQE.2014.2341573

[6] Gao S., Niu H.J., Li Z., Fan X.Y., Duan X.F., Huang Y.Q., *Near-infrared integrated single-wavelength waveguide photodetector under zero bias*, Journal of Liaocheng University (Natural Science Editions) **36**(5), 2023: 49-55 (in Chinese).

[7] Ishibashi T., Kodama S., Shimizu N., Furuta T., *High-speed response of uni-traveling-carrier photodiodes*, Japanese Journal of Applied Physics **36**(10R), 1997: 6263. https://doi.org/10.1143/JJAP.36.6263

[8] Ito H., Furuta T., Kodama S., Ishibashi T., *InP/InGaAs uni-travelling-carrier photodiode with 310 GHz bandwidth*, Electronics Letters **36**(21), 2000: 1809-1810. https://doi.org/10.1049/el:20001274

[9] Wu Y.S., Shi J.W., Chiu P.H., *Analytical modeling of a high-performance near-ballistic uni-traveling-carrier photodiode at a 1.55 μm wavelength*, IEEE Photonics Technology Letters **18**(8), 2006: 938-940. https://doi.org/10.1109/LPT.2006.873567

[10] Wu Y.S., Shi J.W., *Dynamic analysis of high-power and high-speed near-ballistic unitraveling carrier photodiodes at W-band*, IEEE Photonics Technology Letters **20**(13), 2008: 1160-1162. https://doi.org/10.1109/LPT.2008.925195

[11] Li Z., Pan H.P., Chen H., Beling A., Campbell J.C., *High-saturation-current modified uni-traveling-carrier photodiode with cliff layer*, IEEE Journal of Quantum Electronics **46**(5), 2010: 626-632. https://doi.org/10.1109/JQE.2010.2046140

[12] Xiong B., Chao E.F., Luo Y., Sun C.Z., Han Y.J., Wang J., Hao Z.B., Wang L., Li H.T., *Research on ultra-wideband and high saturation power uni-traveling-carrier photodetectors*, Infrared and Laser Engineering **50**(7), 2021: 20211052. https://doi.org/10.3788/IRLA20211052

[13] Du J.W., Wang X.J., Huang Y.Q., Wang S.Y., Yang M.X., Duan X.F., Liu K., Yang Y.S., Ren X.M., *Cascade uni-traveling-carrier photodetector array for terahertz applications*, IEEE Journal of Quantum Electronics **59**(1), 2023: 4400107. https://doi.org/10.1109/JQE.2022.3233091

[14] Huang Y.C., Chen N.W., Wu Y.K., Naseem., Shi J.W., *Improvements in the maximum THz output power and responsivity in near-ballistic uni-traveling-carrier photodiodes with an undercut collector*, Journal of Lightwave Technology **42**(7), 2024: 2362-2370. https://doi.org/10.1109/JLT.2023.3340502

[15] Duan X.F., Wang J.C., Huang Y.Q., Liu K., Shang Y.F., Zhou G.R., Ren X.M., *Mushroom-mesa photodetectors using subwavelength gratings as focusing reflectors*, IEEE Photonics Technology Letters **28**(20), 2016: 2273-2276. https://doi.org/10.1109/LPT.2016.2591955

[16] Kang C., Huang Y.Q., Liu F., Fei J.R., Chen Q.T., Liu K., Duan X.F., Wang Q., Wang J., Zhang X., Ren X.M., *A mushroom dual-absorption partially depleted absorber photodetector*, [In] *Asia Communications and Photonics Conference 2015*, C. Lu, J. Luo, Y. Ji, K. Kitayama, H. Tam, K. Xu, P. Ghiggino, N. Wada, [Eds.], OSA Technical Digest (online), Optica Publishing Group, 2015: ASu2A.1. https://doi.org/10.1364/ACPC.2015.ASu2A.1

[17] Wang J.C., Duan X.F., Huang Y.Q., Liu K., Fei J.R., Chen Q.T., Ren X.M., *Novel 1.55 μm mushroom-type vertical-illumination photodiode*, [In] *Asia Communications and Photonics Conference 2016*, OSA Technical Digest (online), Optica Publishing Group, 2016: AF2A.68. https://doi.org/10.1364/ACPC.2016.AF2A.68

[18] Kato K., Kozen A., Muramoto Y., Itaya Y., Nagatsuma T., Yaita M., *110-GHz, 50%-efficiency mushroom-mesa waveguide p-i-n photodiode for a 1.55-μm wavelength*, IEEE Photonics Technology Letters **6**(6), 1994: 719-721. https://doi.org/10.1109/68.300173

[19] Zhang K.R., Huang Y.Q., Duan X.F., *Design and analysis of hybrid integrated high-speed mushroom vertical PIN photodetector*, Applied Mechanics and Materials **411-414**, 2013: 1455-1458. https://doi.org/10.4028/www.scientific.net/AMM.411-414.1455

[20] EI-BATAWY Y.M., DEEN M.J., *Analysis, circuit modeling, and optimization of mushroom waveguide photodetector (mushroom-WGPD)*, Journal of Lightwave Technology **23**(1), 2005: 423-431. https://doi.org/10.1109/JLT.2004.834483

[21] EI-BATAWY Y.M., DEEN M.J., *Modeling of mushroom waveguide photodetector*, Journal of Vacuum Science and Technology A **22**(3), 2004: 811-815. https://doi.org/10.1116/1.1730328

[22] LIU T., HUANG Y.Q., WEI Q., LIU K., DUAN X.F., REN X.M., *Optimized uni-traveling carrier photodiode and mushroom-mesa structure for high-power and sub-terahertz bandwidth under zero- and low-bias operation*, Journal of Physics Communications **3**(9), 2019: 095004. https://doi.org/10.1088/2399-6528/ab3b70

[23] WANG H.Z., NIU H.J., JIANG C.X., FAN X.Y., FANG W.J., ZHANG X., *A novel dual-absorption photodetector with high bandwidth-efficiency-product*, [In] *2021 Asia Communications and Photonics Conference (ACP)*, Shanghai, China, 2021.

[24] LI Q.L., LI K.J., FU Y., XIE X.J., YANG Z.Y., BELING A., CAMPBELL J.C., *High-power flip-chip bonded photodiode with 110 GHz bandwidth*, Journal of Lightwave Technology **34**(9), 2016: 2139-2144. https://doi.org/10.1109/JLT.2016.2520826

[25] CHEN Q.T., HUANG Y.Q., DUAN X.F., LIU F., KANG C., WANG Q., *High-speed uni-traveling-carrier photodetector with the new design of absorber and collector*, [In] 2015 Opto-Electronics and Communications Conference (OECC), Shanghai, China, 2015. https://doi.org/10.1109/OECC.2015.7340268

[26] DENG J., BURASA P., WU K., *Self-contained dual-input interferometric receiver for paralleled-multichannel wireless systems*, IEEE Transactions on Circuits and Systems I: Regular Papers **71**(2), 2024: 934-947. https://doi.org/10.1109/TCSI.2023.3338214

[27] DENG J., BURASA P., WU K., *Joint multiband linear interferometric receiver for integrated microwave and terahertz sensing and communication systems*, IEEE Transactions on Microwave Theory and Techniques **72**(9), 2024: 5550-5562. https://doi.org/10.1109/TMTT.2024.3363173

[28] SEEDS A.J., SHAMS H., FICE M.J., RENAUD C.C., *Terahertz photonics for wireless communications*, Journal of Lightwave Technology **33**(3), 2015: 579-587. https://doi.org/10.1109/JLT.2014.2355137

[29] SENGUPTA K., NAGATSUMA T., MITTLEMAN D.M., *Terahertz integrated electronic and hybrid electronic –photonic systems*, Nature Electronics **1**, 2018: 622-635. https://doi.org/10.1038/s41928-018-0173-2

[30] DENG J., BURASA P., WU K., *All-in-one dual-polarization waveguide receiver for multichannel wireless systems*, IEEE Transactions on Microwave Theory and Techniques **72**(8), 2024: 4998-5013. https://doi.org/10.1109/TMTT.2024.3355306

[31] GUO L.Q., HUANG Y.Q., DUAN X.F., REN X.M., WANG Q., ZHANG X., *High-speed modified uni-traveling-carrier photodiode with a new absorber design*, Chinese Optics Letters **10**(s1), 2012: S12301 -312304 (in Chinese).

[32] GASPARYAN F.V., AROUTIOUNIAN V.M., ABRAHAMIAN YU.A., VAHANIAN A.I., *Thermoelectric coefficient of the non-homogeneously doped p–n junctions made on Si and* $Pb_{0.8}Sn_{0.2}Te$, Sensors and Actuators A: Physical **113**(3), 2004: 370-375. https://doi.org/10.1016/j.sna.2004.03.047

[33] CHTIOUI M., LELARGE F., ENARD A., POMMEREAU F., CARPENTIER D., MARCEAUX A., VAN DIJK F., ACHOUCHE M., *High responsivity and high power UTC and MUTC GaInAs-InP photodiodes*, IEEE Photonics Technology Letters **24**(4), 2012: 318-320. https://doi.org/10.1109/LPT.2011.2177965

[34] LI X.W., LI N., DEMIGUEL S., ZHENG X.G., CAMPBELL J.C., TAN H.H., JAGADISH C., *A partially depleted absorber photodiode with graded doping injection regions*, IEEE Photonics Technology Letters **16**(10), 2004: 2326-2328. https://doi.org/10.1109/LPT.2004.834563

[35] JIANG C.X., NIU H.J., WANG H.Z., FAN X.Y., FANG W.J., ZHANG X., BAI C.L., *A low-bias operational MPDA photodetector with high bandwidth-efficiency product and high saturation characteristics*, Journal of Modern Optics **69**(11), 2022: 628-634. https://doi.org/10.1080/09500340.2022.2071495

[36] CHEN Q.T., ZHANG X.P., SHARAWI M.S., KASHYAP R., *Advances in high–speed, high–power photodiodes: From fundamentals to applications*, Applied Sciences **14**(8), 2024: 3410. https://doi.org/10.3390/app14083410

[37] KATO K., *Ultrawide-band/high-frequency photodetectors*, IEEE Transactions on Microwave Theory and Techniques **47**(7), 1999: 1265-1281. https://doi.org/10.1109/22.775466

[38] NIU H.J., HUANG Y.Q., YANG Y.S., LIU K., DUAN X.F., WU G., LIU T., WEI Q., REN X.M., *High bandwidth-efficiency product MPIN photodiode with parallel-connected microstructure*, IEEE Journal of Quantum Electronics **56**(5), 2000: 4400305. https://doi.org/10.1109/JQE.2020.3004130

[39] CHEN D., YU X.C., WANG P.H., LIU Y., *Study of the Influence of cliff layer on uni-traveling-carrier photodetector*, Chinese Journal of Lasers **41**(3), 2014: 266-271 (in Chinese).

[40] LI N., LI X.W., DEMIGUEL S., ZHENG X.G., CAMPBELL J.C., TULCHINSKY D.A., WILLIAMS K.J., ISSHIKI T.D., KINSEY G.S., SUDHARSANSAN R., *High-saturation-current charge-compensated InGaAs-InP uni-traveling-carrier photodiode*, IEEE Photonics Technology Letters **16**(3), 2004: 864-866. https://doi.org/10.1109/LPT.2004.823773

[41] ITO H., KODAMA S., MURAMOTO Y., FURUTA T., NAGATSUMA T., ISHIBASHI T., *High-speed and high-output InP–InGaAs unitraveling-carrier photodiodes*, IEEE Journal of Selected Topics in Quantum Electronics **10**(4), 2004: 709-727. https://doi.org/10.1109/JSTQE.2004.833883

[42] ZHEN Z., HAO R., XING D., FENG Z.H., JIN S.Z., *Nearly-ballistic optimization design of high-speed uni-traveling-carrier photodiodes*, Chinese Journal of Lasers **47**(10), 2020: 1006003 (in Chinese).

[43] SMITH P.M., INOUE M., FREY J., *Electron velocity in Si and GaAs at very high electric fields*, Applied Physics Letters **37**(9), 1980: 797-798. https://doi.org/10.1063/1.92078

[44] ISHIBASHI T., *Nonequilibrium electron transport in HBTs*, IEEE Transactions on Electron Devices **48**(11), 2001: 2595-2605. https://doi.org/10.1109/16.960386

[45] CHEN Q.T., HUANG Y.Q., ZHANG X.P., DUAN X.F., FEI J.R., MA X.K., LIU T., WU G., LIU K., REN X.M., *Uni-traveling-carrier photodetector with high-reflectivity DBR mirrors*, IEEE Photonics Technology Letters **29**(14), 2017: 1203-1206. https://doi.org/10.1109/LPT.2017.2712627

[46] LIU F, HUANG Y.Q., KANG C., CHEN Q.T., DUAN X.F., REN X.M., *High speed and high responsivity dual-absorption InGaAs/InP UTC-PDs*, [In] *2015 Opto-Electronics and Communications Conference (OECC)*, Shanghai, China, 2015. https://doi.org/10.1109/OECC.2015.7340304

[47] GAO Y., CANSIZOGLU H., POLAT K.G., GHANDIPARSI S., KAYA A., MAMTAZ H.H., MAYET A.S., WANG Y., ZHANG X., YAMADA T., DEVINE E.P., ELREFAIE A.F., WANG S.Y., ISLAM M.S., *Photon-trapping microstructures enable high-speed high-efficiency silicon photodiodes*, Nature Photonics **11**, 2017: 301-308. https://doi.org/10.1038/nphoton.2017.37

[48] NIU H.J., HUANG Y.Q., YANG Y.S., LIU K., DUAN X.F., CAI S.W., WEI Q., WU G., XIAO C.Z., ZHI H.Y., REN X.M., *Design of the microstructure parallel-connected PIN photodetector with high bandwidth -efficiency product*, [In] *2020 Conference on Lasers and Electro-Optics (CLEO)*, San Jose, CA, USA, 2020.

[49] CHEN Q.T., FANG W.J., HUANG Y.Q., DUAN X.F., LIU K., SHARAWI M.S., REN X.M., *Uni-traveling -carrier photodetector with high-contrast grating focusing-reflection mirrors*, Applied Physics Express **13**(1), 2020: 016503. https://doi.org/10.7567/1882-0786/ab5b4a

[50] WANG H.Z., NIU H.J., JIANG C.X., FANG W.J., FAN X.Y., ZHANG X., BAI C.L., *Symmetric photodetector integrated with multilayer dielectric resonator cavity for 400Gb/s optical communication system*, Results in Optics **9**, 2022: 100324. https://doi.org/10.1016/j.rio.2022.100324

[51] CHEN Q.T., FANG W.J., HUANG Y.Q., DUAN X.F., LIU K., SHARAWI M.S., REN X.M., *High focusing-reflection subwavelength gratings with uni-traveling-carrier photodetector for high responsivity*, [In] *2019 Asia Communications and Photonics Conference (ACP)*, Chengdu, China, 2019.

[52] ZHANG S.Y., NIU H.J., JIANG C.X., LIU T., CHEN Q.T., BAI C.L., *Responsivity enhancement using Fabry-Pérot cavity for zero-bias waveguide photodiodes*, [In] *2024 Asia Communications and Photonics Conference (ACP) and International Conference on Information Photonics and Optical Communications (IPOC)*, Beijing, China, 2024. https://doi.org/10.1109/ACP/IPOC63121.2024.10809851

[53] NIU H.J., ZHANG S.Y., JIANG C.X., LIU T., CHEN Q.T., WEI J., GAO S., HUANG Y.Q., DUAN X.F., BAI C.L., *High-responsivity, high-power waveguide photodetector with Fabry-Pérot cavity and quasi-dipole doping for sub-THz applications*, Optics Communications **577**, 2025: 131412. https://doi.org/10.1016/j.optcom.2024.131412

[54] NIU H.J., HUANG Y.Q., YANG Y.S., XIAO C.Z., YUAN W.F., ZHI H.Y., DUAN X.F., LIU K., REN X.M., *Influence of the incident optical field distribution on a high-speed PIN photodetector and horizontal optimization*, Applied Optics **60**(3), 2021: 727-734. https://doi.org/10.1364/AO.411439

[55] LIU T, HUANG Y.Q., FEI J.R., CHEN Q.T., MA X.K., DUAN X.F., LIU K., REN X.M., *Influences of contact electrode shape and incidence direction on p-i-n photodiodes*, IET Optoelectronics **13**(4), 2019: 151-154. https://doi.org/10.1049/iet-opt.2018.5037

[56] WEI J., NIU H.J., CHEN Q.T., LI Y.H., LIU K., DUAN X.F., HUANG Y.Q., *Research on PIN photodetector with novel low-loss electrode*, Journal of Liaocheng University (Natural Science Editions) **38**(1), 2025: 23-33 (in Chinese).

[57] SHIMIZU N., WATANABE N., FURUTA T., ISHIBASHI T., *Improved response of uni-traveling-carrier photodiodes by carrier injection*, Japanese Journal of Applied Physics **37**(3S), 1998: 1424. https://doi.org/10.1143/JJAP.37.1424

[58] ISHIBASHI T., FURUTA T., FUSHIMI H., ITO H., *Photoresponse characteristics of uni-traveling-carrier photodiodes*, Proceedings of the SPIE, Vol. 4283, Physics and Simulation of Optoelectronic Devices IX: 2001. https://doi.org/10.1117/12.432597

[59] WILLIAMS K.J., ESMAN R.D., WILSON R.B., KULICK J.D., *Differences in p-side and n-side illuminated p-i-n photodiode nonlinearities*, IEEE Photonics Technology Letters **10**(1), 1998: 132-134. https://doi.org/10.1109/68.651136

Received October 27, 2024
in revised form January 11, 2025